Received 24 May 2023; revised 10 July 2023; accepted 19 July 2023. Date of publication 25 July 2023; date of current version 10 August 2023.

Digital Object Identifier 10.1109/OJAP.2023.3298773

Design of a Compact 4-Element GNSS Antenna Array With High Isolation Using a Defected Ground Structure (DGS) and a Microwave Absorber

ABDULLAH MADNI[1] AND WASIF TANVEER KHAN[1,2] (Senior Member, IEEE)

[1]Syed Babar Ali School of Science and Engineering, Lahore University of Management Sciences, Lahore 54792, Pakistan

[2]School of Electrical Engineering and Computer Science, National University of Sciences and Technology, Islamabad 44000, Pakistan

CORRESPONDING AUTHOR: A. MADNI (e-mail: 19060037@lums.edu.pk)

ABSTRACT This work presents a compact (125 mm diameter) wideband 4-element antenna array with a high isolation level for global navigation satellite system (GNSS) applications. The array consists of four right hand circularly polarized (RHCP) single feed rectangular patch antennas that can cover BeiDou B1 band (1561.098 MHz), GPS L1 band (1575.42 MHz), Galileo E1 band (1575.42 MHz) and GLONASS G1 band (1602 MHz) of the GNSS upper L-band (1559 - 1610 MHz). The proposed array has a wide frequency bandwidth of 80 MHz with an axial ratio of less than 3 dB. The patch elements are designed on a substrate which has a high dielectric constant to achieve a compact size. A novel defected ground structure (DGS) has been introduced in the ground plane along with a MT-30 microwave absorber on the top of the array to achieve a high isolation of more than 25 dB in the entire band of interest. The proposed design has a radiation efficiency of more than 58.8% and a peak gain of 6 dBi.

INDEX TERMS Antenna array, circularly polarized, global navigation satellite system, high isolation.

I. INTRODUCTION

DURING the last few decades, global navigation satellite system (GNSS) such as GPS, BeiDou and GLONASS have developed significantly. Circularly polarized (CP) microstrip patch antenna is a judicious choice for GNSS systems due to its various advantages such as immunity to faraday rotation, low profile, low cost and simplicity in the fabrication process using modern printed circuit technology [1], [2]. However, due to an increasingly contaminated electromagnetic environment, GNSS systems often suffer from weak signal levels and are vulnerable to jamming and interference. To mitigate these undesirable effects most GNSS systems employ anti-jamming antenna arrays. These arrays use multiple antenna elements to create nulls in the direction of jammers so that the array can still receive the signal in the other directions. In addition to the anti-jamming capability, it is desirable to have miniaturized and compact antenna arrays for mounting them on vehicles and aircrafts. This requires the antennas to be compact in size and placed closely to each other to reduce the overall array size. It is also a common practice to use thick substrates to achieve enhanced bandwidth. An important parameter to consider when designing multi-element antennas is the mutual coupling between them. If antennas are packed densely to achieve a compact array size, this leads to higher mutual coupling between them due to their close proximity. On the other hand, due to the presence of the surface waves in thicker substrates, mutual coupling is greatly enhanced. An obvious technique to mitigate mutual coupling is to increase the inter-element separation. However, this method is vulnerable to the grating lobes that are formed when the spacing between the elements is a multiple of wavelength [1], [3]. Furthermore, increasing the inter-element distance will lead to a larger array size which is undesirable for many applications. In GNSS arrays, high mutual coupling is extremely undesirable as it degrades the radiation efficiency and null depth [4].

Various techniques have been proposed to address the issue of mutual coupling in patch antennas as in [5] microstrip antennas have been designed to reduce surface waves by introducing additional coupling path such that the dominant mode is not excited resulting in reduced mutual coupling.

However, this method is limited to only specific antenna types. Another method involves the cancellation of mutual coupling by introducing an inductive or capacitive equal and opposite coupling but this technique has narrow band coupling suppression [5], [6].

Another popular approach to mitigate mutual coupling involves the use of electromagnetic band-gap (EBG) structures. These EBG structures exhibit band-stop characteristics for surface wave propagation thereby reducing the mutual coupling between the array elements. In one of such works, a mushroom like EBG structure is proposed to reduce mutual coupling in E- and H-coupled antennas to about –24 dB [7]. Similarly, in another work an EBG structure is proposed for an E-plane aligned 4 x 1 microstrip antenna array [8]. EBG structures also have been used in multilayer dielectric substrates for mutual coupling reduction [9]. Nonetheless, most of the EBG structures often comprise complex geometry involving vias making the overall occupied area larger and the fabrication process difficult. Furthermore, EBGs give a narrow band isolation level making their utility limited.

Recently, metamaterials have gained a lot of popularity due to their unconventional behavior and compact size. These are artificially engineered materials and exhibit negative permeability within the vicinity of their resonant frequencies. They have simpler geometries and hence are easier to fabricate as compared to the EBG structures. Metamaterials such as split ring resonators (SRRs) and complementary split ring resonators (CSRRs) have been employed successfully to demonstrate mutual coupling reduction in antenna arrays. In [10], an open slot SRR has been proposed to reduce mutual coupling between two closely placed patch antenna resulting in an isolation enhancement of 6.5 dB. Similarly, in [11] a CSRR has been incorporated to suppress the mutual coupling for a four-port antenna. Metamaterials also have been employed as insulating walls as in [12] where a wall of vertically placed metamaterial is designed to reduce mutual coupling lower than -20 dB. Similar type of vertically placed resonators also has been used in [13] to alleviate the mutual coupling in a compact 2 × 2 GPS array. However, a major disadvantage of these two designs is their complex fabrication and assembling due to the vertical arrangement of SRRs. Moreover, they are not desirable for applications involving vibrations such as aircrafts and high-speed vehicles. Furthermore, SRRs are polarization sensitive and their decoupling performance is dependent on their orientation with respect to the magnetic field component. Hence, they are more suitable in linearly polarized antennas as GNSS antennas are circularly polarized and exhibit complex coupling mechanism due to the simultaneous existence of two orthogonal modes [14].

Another popular method for increasing isolation in MIMO antennas is the use of defected ground structures (DGS). These structures act as *LC* resonant networks. When these structures are etched in the ground plane, they act as band-stop filters and increase the isolation level between the antennas. Many works have been published employing DGS as in [15] a fractal defected ground structure (FDGS) is introduced in a two-port MIMO antenna to enhance the isolation level. Various other geometries of DGS structures have been reported in [16], [17] to increase the isolation level in MIMO antennas. An advantage of DGS is that it doesn't affect the polarization of antennas as compared to metamaterials. Furthermore, as compared to EBGs the fabrication of DGS is easier.

In this work, we propose a compact (125 mm diameter) circular 4-element antenna array for GNSS applications. As compared to the previously reported works that cover only one or two GNSS bands and require complex fabrication process, our proposed antenna employs a hybrid approach consisting of a DGS and a microwave absorber material to cover all the four GNSS services (BeiDou, GPS, Galileo, GLONASS) in the upper L-band with a high isolation level. The proposed antenna design consists of four coaxial feed circularly polarized rectangular patches designed on a high epsilon material to achieve a compact size. To achieve a high isolation level (> 17 dB), a novel DGS structure is etched in the ground plane. Furthermore, we also have placed a thin MT-30 microwave absorber material to further enhance the isolation level to more than 25 dB. Similar types of absorbers have been used for mutual coupling suppression as in [18] Eccosorb AN-79 has been used for isolation in full-duplex wireless communication systems. However, MT-30 absorber is lighter in weight and less expensive as compared to Eccosorb AN-79 [19]. This work builds upon the previous work reported in [19] where a 9.525 mm thick MT-30 absorber has been used to achieve 20 dB isolation in a four element array having the same 125 mm diameter. Despite having a good isolation level, the design suffers from poor efficiency (38% only) and gain (3.3 dBi only) due to the presence of a thick absorber. Our proposed design achieves high isolation of more than 25 dB without degrading the radiation efficiency and gain by utilizing a novel defected ground structure along with a 3.175 mm thick absorber which is only placed at the center of the array instead of around the radiating patches as reported in [19]. Our proposed approach allows us to achieve a gain of 6 dBi and an efficiency of more than 58% while maintaining an isolation of more than 25 dB. To the best of our knowledge, the proposed array covers all the GNSS services of the upper L-band with the highest isolation level reported within a compact diameter of only 125 mm (area = 122.65 cm^2).

Following this introduction, rest of the paper is organized as follows: Section II explains the design process and simulated results of our proposed antenna array while Section III presents the antenna fabrication and measured results. Finally, a conclusion is presented in the last section.

II. FOUR ELEMENT GNSS ARRAY DESIGN PROCESS

A. SIMPLE FOUR ELEMENT ANTENNA ARRAY DESIGN

Initially, a simple four-element antenna array was simulated without any decoupling structure having a complete

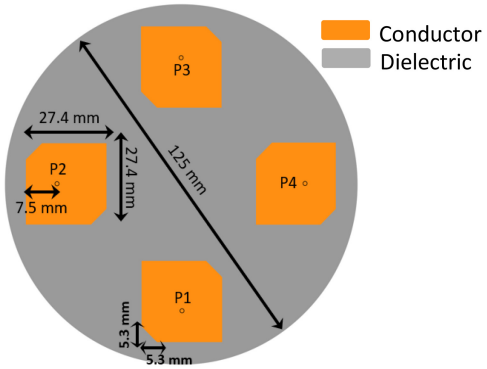

FIGURE 1. Design geometry of a simple four-element GNSS antenna array on TMM10i.

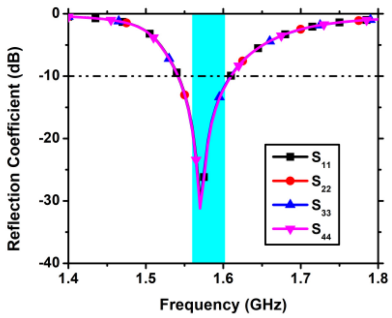

FIGURE 2. Simulated impedance matching response of simple four element GNSS antenna array.

ground plane. The design geometry consisted of four rectangular patches with truncated opposite corners placed on a circular Rogers TMM10i substrate ($\varepsilon_r = 10.5$, $\tan\delta = 0.0020$) having a diameter of 125 mm and a thickness of 5.08 mm. The four patches are placed in a sequentially rotated architecture and this arrangement has also been used to generate circular polarization (CP) from linearly polarized antennas [19]. This symmetrical arrangement is preferred as two antenna elements on each opposite axis allow us to form *N-1* nulls, where *N* is the number of antenna elements [19]. As the antenna elements were sequentially rotated, therefore the ports are fed by P1 = 0°, P2 = 90°, P3 = 180° and P4 = 270° phases to achieve RHCP gain pattern without any nulls. The antenna is modelled using High Frequency Structure Simulator (HFSS). Fig. 1 shows the proposed simple four-element array design geometry.

Overall, the mutual coupling in the entire bandwidth of interest is less than −11 dB. To further identify the regions of high mutual coupling, the surface current distribution is shown.

The simulated impedance response of the proposed simple four element antenna array is shown in Fig. 2. The bandwidth being covered is from 1.54 to 1.61 GHz.

It can be seen that when element 1 is excited, the surface current is highly coupled with element 2 and 4 as they are very close to the radiating patch. Patch 3 is situated at greater distance from the radiating patch so the isolation between them is good, i.e., more than 20 dB (Fig. 3). Due

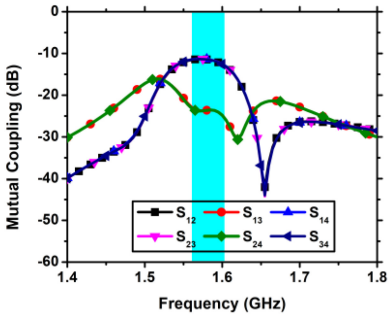

FIGURE 3. Simulated mutual coupling of simple four element GNSS antenna array.

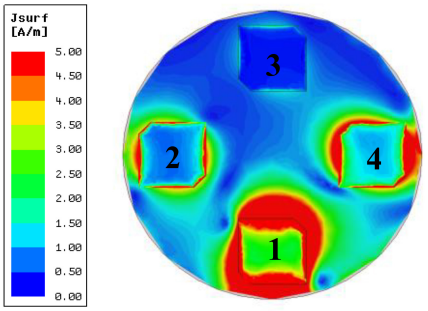

FIGURE 4. Simulated surface current distribution of four element array at 1.575 GHz.

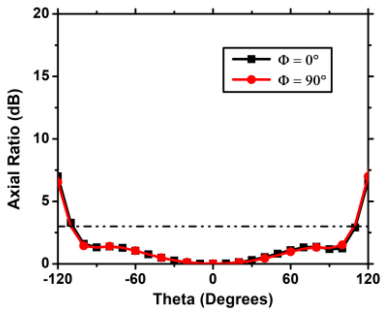

FIGURE 5. Simulated axial ratio of simple four element GNSS antenna array.

to a symmetrical design geometry, exciting the other ports generates the similar effect. To increase the isolation between the adjacent antenna elements a defected ground structure (DGS) is incorporated in the ground plane.

The axial ratio of the proposed simple array is shown in Fig. 5 as a function of the polar angle at 1.575 GHz. It is less than 3 dB with a beamwidth of about 180° for good CP performance.

The simulated mutual coupling response is shown in Fig. 3. The mutual coupling of the proposed four element antenna can be divided into two categories, i.e., coupling between the adjacent antenna elements (S_{12}, S_{14}, S_{23}, S_{34}) and the coupling between the opposite elements (S_{13}, S_{24}). Furthermore, due to symmetrical design geometry $S_{12} = S_{21}$, $S_{13} = S_{31}$ and so on.

The mutual coupling between the adjacent elements is less than –11 dB due to their close proximity (Fig. 3) while for the opposite elements the coupling is less than –20 dB.

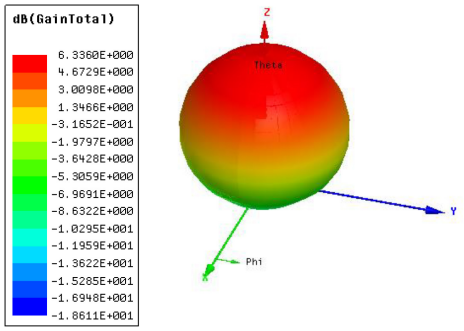

FIGURE 6. Simulated 3D radiation pattern of simple four element array.

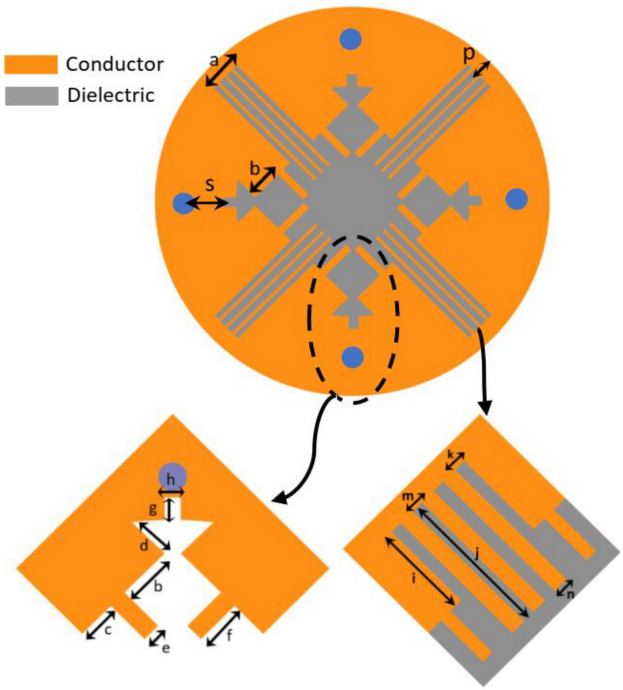

FIGURE 7. Design geometry of the proposed 4-element antenna array with DGS.

The 3D radiation pattern of the proposed array at 1.575GHz is shown in Fig. 6.

B. FOUR ELEMENT ANTENNA ARRAY WITH DGS

In order to increase the isolation level of the four element antenna array shown in Fig. 1, a modified fork-like defected ground structure (DGS) is employed. Fig. 7 illustrates the design geometry of the proposed DGS.

The simulated reflection coefficient of the proposed structure is shown in Fig. 8.

The simulated mutual coupling response is shown in Fig. 9. It can be observed that the mutual coupling is less than −17 dB in the entire bandwidth of interest. Hence there is an improvement of 6 dB in the isolation level after incorporating the proposed DGS. Table 1 shows the optimized design parameters of the proposed DGS.

The step-by-step process that led to the development of the proposed DGS involves initially cutting a circular slot

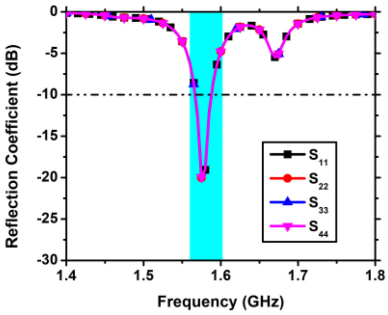

FIGURE 8. Simulated impedance response of four-element GNSS antenna array with DGS.

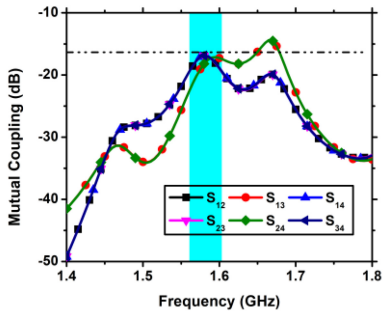

FIGURE 9. Simulated mutual coupling of four-element GNSS antenna array with DGS.

TABLE 1. Optimized design parameters of DGS.

Parameter	Value (mm)	Parameter	Value (mm)	Parameter	Value (mm)
a	9.85	*f*	11.48	*k*	1.42
b	11.46	*g*	4.03	*m*	2.1
c	3.55	*h*	3	*n*	0.9
d	6.74	*i*	36	*p*	3.67
e	2	*j*	42	*s*	3

in the ground plane of the simple four-element array. In the next step, rectangular perturbations are added at the diagonal positions. Finally, in the last step, a fork-shaped DGS is added along with some slots and stubs near the ports (Fig. 7) so that an isolation level of more than 17 dB is achieved in the band of interest. Fig. 10 shows the step-by-step ground plane evolution of the proposed four-element antenna array with DGS only.

The mutual coupling response of each ground plane stage is illustrated in Fig. 11.

The antenna array with ground-1 exhibits an isolation level of only 13 dB which is increased to more than 15 dB by modifying it to ground-2. Ground-3 consists of a fork-shaped DGS to further enhance the isolation level to more than 17 dB in the entire band of interest. The corresponding reflection coefficients of these cases are shown in Fig. 12.

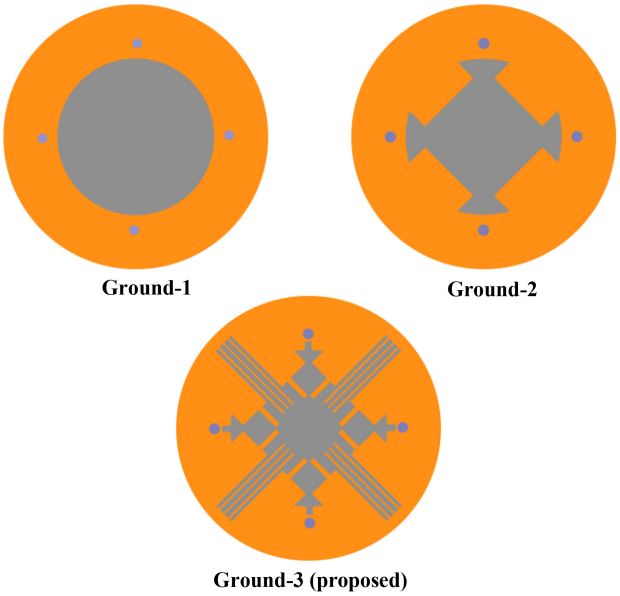

FIGURE 10. Step-by-step evolution stages of the ground plane of the proposed DGS only four-element antenna array.

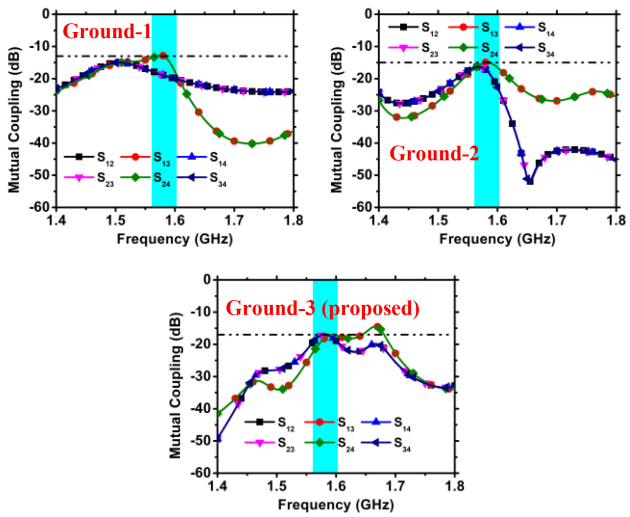

FIGURE 11. Mutual coupling response of each ground plane stage of the proposed DGS based four-element antenna array.

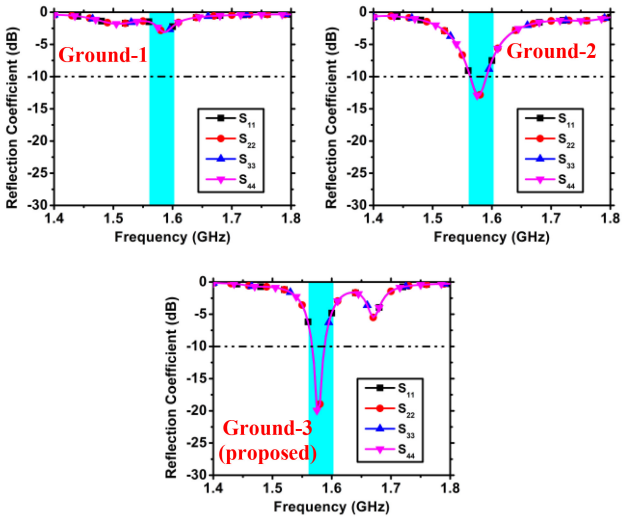

FIGURE 12. Reflection Coefficient of each ground plane stage of the proposed DGS based four-element antenna array.

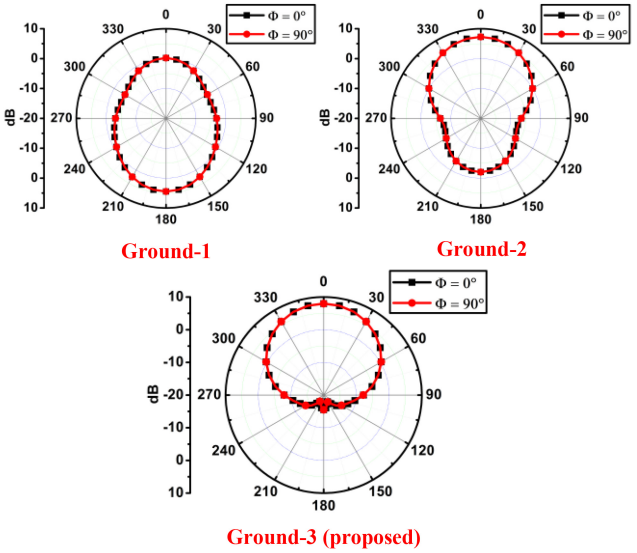

FIGURE 13. 2D radiation pattern of each ground plane stage of the proposed DGS based four-element antenna array.

It can be observed that the reflection coefficient of ground-3 is better than ground-2 and ground-1 with the antenna array resonating at the center frequency which is GPS L1 band, i.e., 1.575 GHz.

The corresponding 2D radiation patterns of these cases are presented in Fig. 13 for the GPS L1 band (1.575 GHz). It can be observed that there is back lobe radiation for ground-1 and ground-2. However, for ground-3 there is no significant back lobe radiation. Therefore, the proposed DGS based four element antenna array (Fig. 7) is covering the full upper half spherical-beam facing the sky which is required for GNSS antenna arrays.

Therefore, the proposed ground-3 based antenna design (Fig. 7) has an isolation level of 17 dB in the entire band of interest without any significant back-lobe radiation. The 3D radiation pattern of the proposed DGS based antenna at 1.575 GHz is shown in Fig. 14 which is in accordance with the 2D radiation pattern of ground-3 shown above.

The axial ratio of the proposed four-element array with the proposed ground 3 (Fig. 7) is shown in Fig. 15. The axial ratio is less than 3 dB for good CP performance with a beamwidth of about 180°.

It can be concluded from the above discussion that the ground plane of the proposed antenna plays a decisive role in the improvement of isolation of the proposed antenna. Apart from isolation, the other important antenna parameters such as axial ratio, gain, and radiation pattern are not degraded. The axial ratio is less than 3 dB (Fig. 15), the gain is more than 6 dBi (Fig. 14) and there is no significant back lobe radiation as observed in Fig. 13. The reflection coefficient of the antenna is slightly degraded after employing DGS but

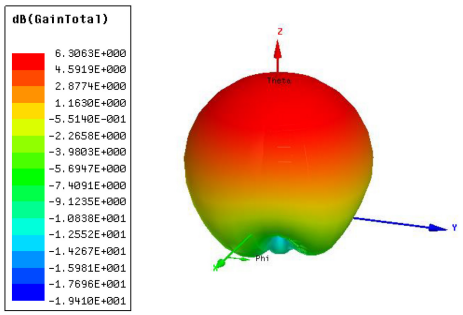

FIGURE 14. Simulated 3D radiation pattern of four element array with DGS.

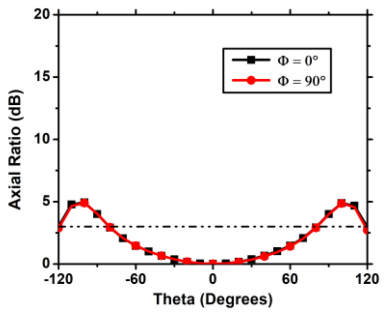

FIGURE 15. Simulated axial ratio of four element GNSS antenna array with DGS (Fig. 7).

it is still resonating at the center frequency of 1.575 GHz (GPS L1 band). In the next step, a microwave absorber is employed which not only improves the isolation level to more than 25 dB but also improves the reflection coefficient.

C. FOUR ELEMENT ANTENNA ARRAY WITH DGS AND ABSORBER

In order to further increase the isolation level, a 3.175 mm thick microwave absorber material MT-30 ($\varepsilon_r = 15.79$, $\tan\delta = 1.944$) is placed on the top surface at the center of the array. The introduction of microwave absorber alters the input impedance of the patches and effects the impedance matching performance. Therefore, we have re-optimized the locations of feed points s, size of patch elements, width of the slot with fork branches a and the distance between the fork-shaped branches m (Fig. 7) in the ground plane of the antenna array to tune the array for optimum performance within our desired bandwidth of interest. Fig. 16 shows the design geometry of the proposed absorber based DGS array.

We have chosen $a = 17$ mm, $s = 6.8$ mm, and $m = 3.35$ mm in our re-optimized ground plane such that the bandwidth as well as the isolation remains satisfactory. Fig. 17 shows the impedance matching response of the proposed array which indicates that all four GNSS bands are occupied.

The simulated mutual coupling response is shown in Fig. 18. The mutual coupling is less than –25 dB in the entire bandwidth of interest. Therefore, there is an improvement of 14 dB in isolation level as compared to the case involving simple four element array (Fig. 1).

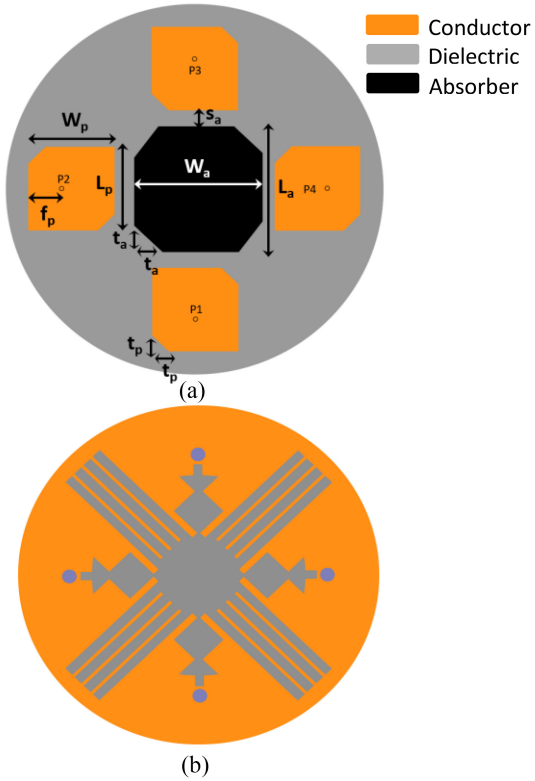

FIGURE 16. Design geometry of the proposed four-element array with absorber and DGS. (a) Top layout with absorber. (b) Bottom layout with DGS.

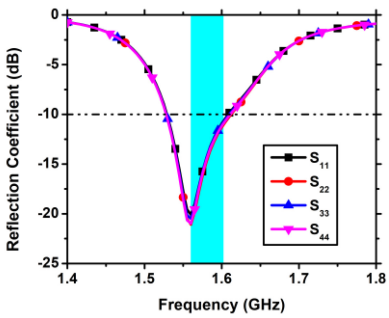

FIGURE 17. Simulated impedance response of four-element GNSS antenna array with DGS and absorber.

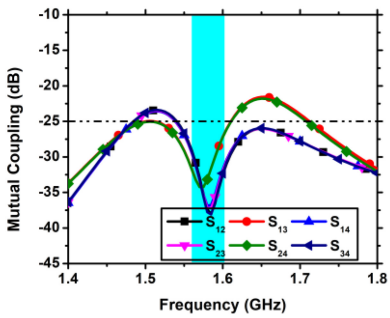

FIGURE 18. Simulated mutual coupling of four-element GNSS antenna array with DGS and absorber.

Table 2 summarizes the isolation enhancement achieved by each technique starting with the simple four element array without any decoupling structure having an isolation level

TABLE 2. Isolation achieved from each technique.

Technique	Isolation (dB)
Simple Array	>11
Array with DGS only	>17
Array with DGS and absorber	>25

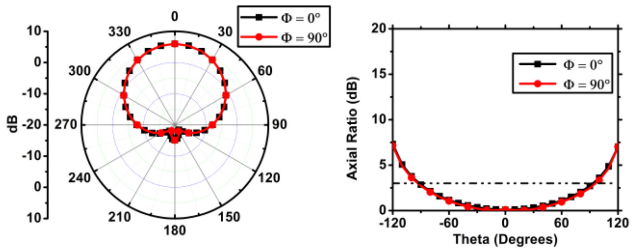

FIGURE 19. Simulated results of the proposed 4-element array with DGS and absorber. (a) 2D radiation pattern (b) axial ratio.

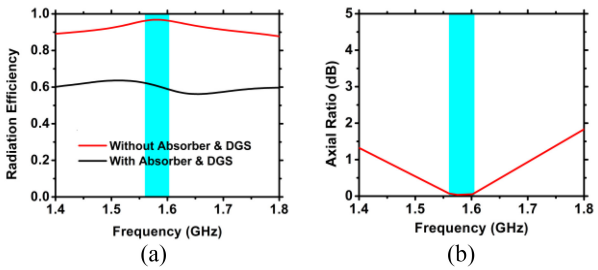

FIGURE 20. Simulated results of the proposed 4-element array with DGS and absorber. (a) radiation efficiency (b) axial ratio variation with frequency.

of only 11 dB. In the second step a DGS was employed to achieve an isolation level of 17 dB. Finally in the last step, a microwave absorber material was incorporated to further enhance the isolation level to 25 dB.

The gain of the proposed array is more than 6 dBi while the axial ratio is less than 3 dB for good CP performance. Fig. 19 illustrates these results for the GPS L1 band (1.57542 GHz). The axial ratio beamwidth is about 180°. Hence, the proposed antenna is able to cover the full upper half spherical beam facing the sky. Furthermore, the axial ratio is also not degraded at the cost of improving the isolation level.

The simulated radiation efficiency of the proposed antenna array and the axial ratio variation with frequency is shown in Fig. 20. The efficiency with both absorber and DGS at BeiDou B1 band (1.561 GHz) is 62.2%. At GPS L1 and Galileo E1 bands (1.57542 GHz), the value of efficiency is 61.2% while at GLONASS G1 band the efficiency is 58.8%. These values of efficiencies are better than reported in [19] by up to a maximum of 24%. The axial ratio is less than 3 dB in the required band of interest.

The impact of microwave absorber on the isolation can be analyzed by the simulating the surface current distribution.

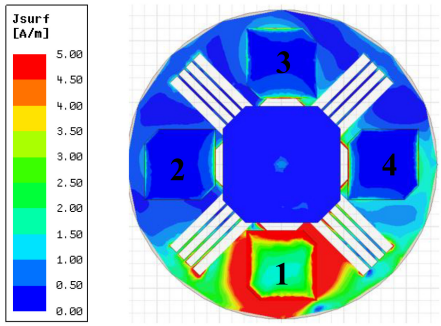

FIGURE 21. Simulated surface current distribution of four element array with DGS and absorber at 1.57542 GHz.

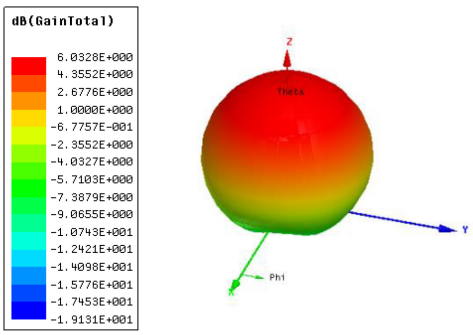

FIGURE 22. Simulated 3D radiation pattern of four element array with DGS and absorber.

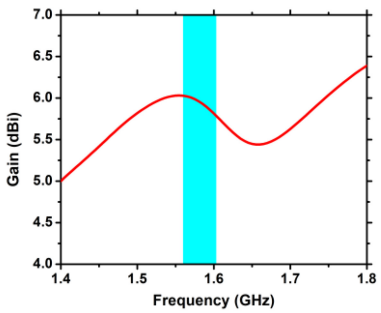

FIGURE 23. Simulated gain vs frequency plot of the proposed four element antenna with DGS and absorber.

Fig. 21 shows the surface current distribution of the absorber based DGS array at the GPS L1 band, i.e., 1.57542 GHz. During these simulations port 1 is excited and the other ports are turned off to analyze the coupling performance. The current is trapped by the fork shaped DGS and the absorber thereby increasing the isolation level.

The 3D radiation pattern of the proposed DGS and absorber based array is shown in Fig. 22 at 1.575 GHz. The array has a peak gain of above 6 dBi. Therefore, there is no significant degradation in gain by using the absorber and DGS as the gain is still more than 6 dBi.

Fig. 23 shows the gain variation of the proposed array with DGS and absorber against frequency. The peak gain is 6 dBi at 1.561 GHz.

The RHCP and left hand circularly polarized (LHCP) gain variation with frequency and polar angle is shown in Fig. 24

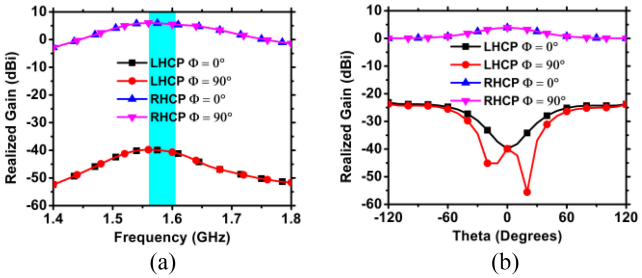

FIGURE 24. Simulated results of the proposed 4-element array with DGS and absorber. (a) realized CP gain variation with frequency (b) realized CP gain variation with theta.

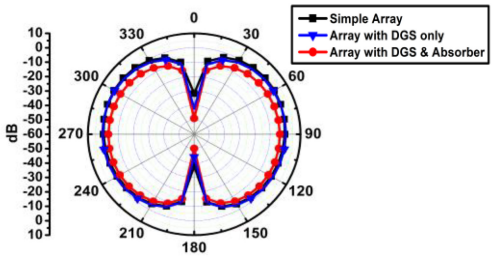

FIGURE 25. Simulated radiation pattern at GPS L1 band with null in the boresight direction.

TABLE 3. Optimized design parameters of DGS and absorber array.

Parameter	Value (mm)	Parameter	Value (mm)
W_p	27.4	L_a	51
L_p	27.4	W_a	51
f_p	8.75	t_a	9
t_p	5.6	-	
s_a	2.1	-	

indicating that our proposed array is RHCP having good polarization purity.

The anti-jamming performance of the proposed antenna array can be evaluated by adding nulls. If each port is fed by a phase shift of 0°, then a null is formed at the boresight direction. Fig. 25 shows the radiation pattern with null formed at the boresight for the simple array, array with DGS only and the array with both DGS and absorber.

The null depth for the simple four-element array is 31 dB, for array with DGS only the null depth is 42 dB and for the array with DGS and absorber the null depth achieved is 48 dB. Therefore, for the design with the highest isolation level (> 25 dB) i.e., array with DGS and absorber the null depth is maximum indicating good anti-jamming performance. Table 3 shows the optimized design parameters of our proposed design (Fig. 16).

The microwave absorber material MT-30 is commercially available in a thickness of 3.175x mm, where x is an integer ranging from 1 to 4. We have chosen x =1 in our proposed

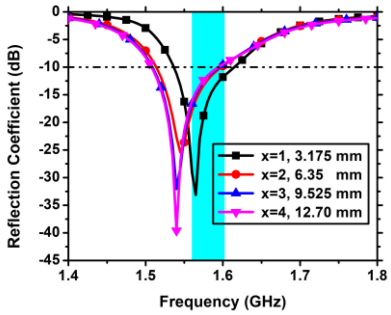

FIGURE 26. Variation in the reflection coefficient of the DGS and absorber antenna with absorber thickness.

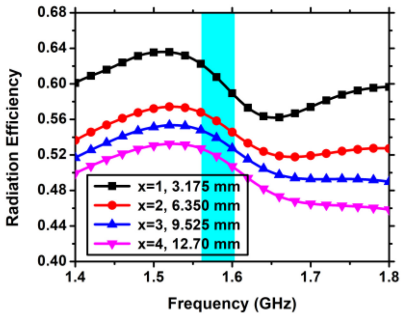

FIGURE 27. Variation in the radiation efficiency of the DGS and absorber antenna with absorber thickness.

design hence the thickness of the absorber being used is 3.175 mm (Fig. 16a). Fig. 26 shows the variation of reflection coefficient of our proposed antenna with increase in the thickness of the absorber. Since our proposed antenna has perfect symmetry and $S_{11} = S_{22} = S_{33} = S_{44}$, hence we have shown the variation of S_{11} only against the standard thickness of the available absorber. Increasing the absorber thickness increases the bandwidth and shifts the impedance response towards the lower end of the frequency spectrum.

It is also important to keep in mind that the radiation efficiency is degraded as the absorber thickness is increased. Fig. 27 shows the effect of increasing the absorber thickness on radiation efficiency.

It can be observed in Fig. 27 that the radiation efficiency is maximum for the absorber with a thickness of 3.175 mm. For the absorber with the highest thickness of 12.70 mm, the radiation efficiency drops to only about 50%. Therefore, in our proposed design we have chosen the least available thickness of the absorber, i.e., 3.175 mm such that the radiation efficiency is not degraded and the required bandwidth is also covered. Furthermore, using the absorber of least available thickness makes our design cost effective and easier to be assembled into a fabricated prototype.

The thickness of the absorber also impacts the isolation level. Since the absorber is placed in the center of the array, therefore it effects the isolation between the opposite antenna elements, i.e., antenna 1 and 3 and antenna 2 and 4 (Fig. 16) significantly as compared to the adjacent antenna elements.

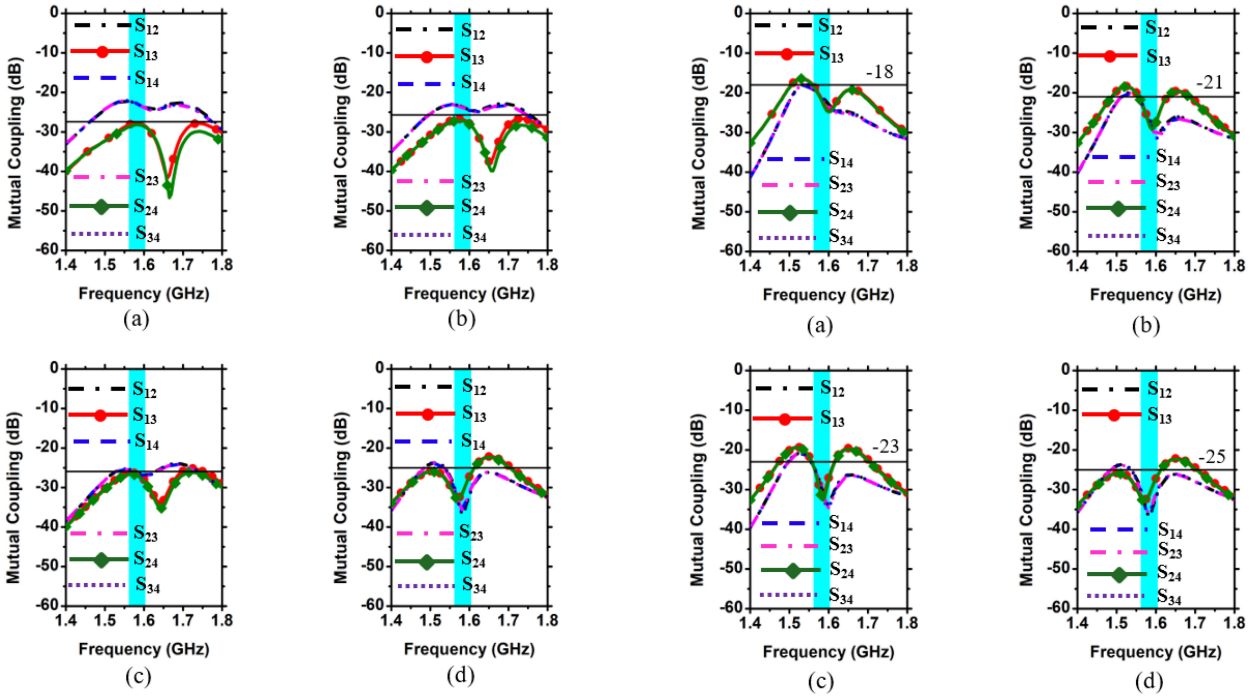

FIGURE 28. Variation of mutual coupling with absorber height (solid lines with symbols for opposite elements S_{13} & S_{24}, dashed lines for adjacent elements S_{12}, S_{14}, S_{23} & S_{34}) at (a) absorber height 12.7 mm and $W_p = L_p = 26$ mm, (b) absorber height 9.525 mm and $W_p = L_p = 26$ mm, (c) absorber height 6.35 mm and $W_p = L_p = 26$ mm (d) absorber height 3.175 mm and $W_p = L_p = 27.4$ mm.

FIGURE 29. Variation of mutual coupling with S_a (solid lines with symbols for opposite elements S_{13} & S_{24}, dashed lines for adjacent elements S_{12}, S_{14}, S_{23} & S_{34}) at (a) $S_a = 10.6$ mm, (b) $S_a = 8.1$ mm, (c) $S_a = 7.1$ mm and (d) $S_a = 2.1$ mm.

As the absorber height is increased isolation between the opposite antenna elements increases.

For the absorber height of 12.7 mm the isolation for opposite elements is more than 28 dB, for absorber height of 9.525 mm the isolation for opposite elements is 27 dB while for 6.35 mm thick absorber it is 26 dB. Since increasing the absorber height also shifts the reflection coefficient as shown in Fig. 26, therefore the size of the patch is slightly reduced to $W_p = L_p = 26$ mm so that during the simulations the required bandwidth of interest is covered. For absorber height of 3.175 mm, the patch size is chosen to be $W_p = L_p = 27.4$ mm so that the required bandwidth is covered and at this height the adjacent as well as the opposite elements have an isolation level of more than 25 dB. Fig. 28 illustrates the variation in isolation level with absorber height.

It is clear from the above simulations that for the absorber height of 3.175 mm, the reflection coefficient, isolation and the radiation efficiency are the most ideal. At this thickness the isolation level of adjacent as well as the opposite elements remains more than 25 dB as shown in Fig. 28d. Using an absorber of height greater than 3.175 mm will not only degrade the radiation efficiency (Fig. 27) but also impact the isolation level of the adjacent antenna elements.

Another critical parameter that affects the isolation of the proposed array is the distance of the absorber form the edges of the patches shown by S_a (Fig. 16a). The isolation level increases as the absorber size W_a is increased, i.e., S_a is reduced. For $S_a = 10.6$ mm, the isolation is more than 18 dB in the bandwidth of interest. As S_a is reduced and the absorber is brought closer to the edges of the antenna patches, the isolation level increases and the at $S_a = 2.1$ mm a high isolation level of more than 25 dB is observed in the entire bandwidth of interest. Fig. 29 illustrates this trend for different values of S_a keeping the absorber height fixed, i.e., 3.175 mm.

The above discussion shows that we have positioned the absorber in such a way that it equally impacts the isolation level for all the antenna elements. The parameters of the absorber have been optimized such that the isolation in the entire bandwidth of interest is more than 25 dB. The height of the absorber is also chosen to be minimum such that the radiation efficiency is not degraded.

The performance of the proposed DGS and absorber based array can also be analyzed by MIMO performance parameters such as the Envelope Correlation Coefficient (ECC) and Diversity Gain (DG). For a two port antenna ECC can be found form the antenna far-fields using the following expression [20]:

$$|\rho_{12}|^2 = \rho_e \text{ (ECC)} = \frac{\left|\iint_{4\pi}[E_1(\theta,\Phi) * E_2(\theta,\Phi)\mathrm{d}\Omega\right|^2}{\iint_{4\pi}|E_1(\theta,\Phi)|^2\mathrm{d}\Omega \iint_{4\pi}|E_1(\theta,\Phi)|^2\mathrm{d}\Omega} \quad (1)$$

The value of ECC for an uncorrelated antenna should be zero ideally, however, ECC below 0.5 is considered good for MIMO performance [20]. Fig. 30 shows the ECC for the proposed four-element DGS and absorber based array which is less than 0.35 in the entire band of interest.

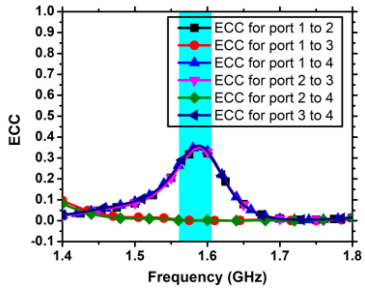

FIGURE 30. ECC of the proposed DGS and absorber based four element antenna array.

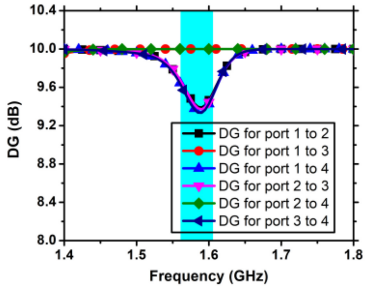

FIGURE 31. DG of the proposed DGS and absorber based four element antenna array.

Another important MIMO parameter is the diversity gain (DG). It can be evaluated from the following expression [20]:

$$\mathrm{DG} = 10\sqrt{(1 - |\rho|^2)} \tag{2}$$

where ρ is the complex correlation coefficient, with $|\rho|^2 \approx$ ECC.

DG for good MIMO performance should be more than 9 dB [20]. Fig. 31 shows the simulated DG for the proposed DGS and absorber based four element array which is more than 9.3 dB in the entire band of interest.

Therefore, it is clear that the proposed DGS and absorber antenna array also has good MIMO performance in the entire bandwidth of interest.

III. FABRICATION AND MEASURED RESULTS

The proposed four-element absorber-based DGS antenna array (Fig. 16) was fabricated by using a LPKF rapid prototype milling machine S103 on Rogers TMM10i substrate. The MT-30 absorber having a thickness of 3.175 mm was also fabricated by using the same machine and is held in fixed position by using two screws. Fig. 32 shows the top and bottom layout of the fabricated antenna array.

The S-parameters of the fabricated model were measured by using a Rhode and Schwarz vector network analyzer (VNA) ZVA 40. Fig. 33 shows the measured impedance matching response of the fabricated antenna array. It is clear from Fig. 30 that the fabricated model covers all the four major GNSS bands, i.e., GPS L1, BeiDou B1, Galileo E1 and GLONASS G1 in the GNSS upper L-band.

It can be observed in Fig. 34 that the mutual coupling in the entire bandwidth of interest is less than −25 dB. The

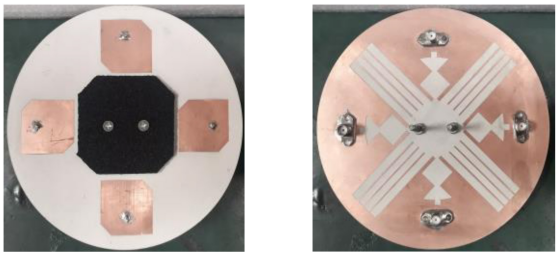

FIGURE 32. Fabricated model of the proposed absorber and DGS based four-element antenna array. (a) Top view (b) Bottom view.

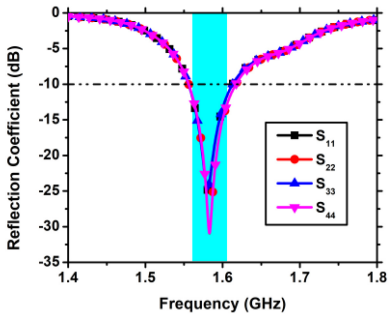

FIGURE 33. Measured impedance matching response of four-element GNSS antenna array with DGS and absorber.

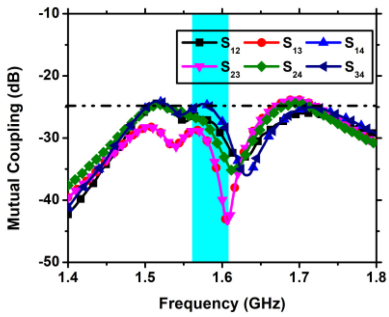

FIGURE 34. Measured mutual coupling of four-element GNSS antenna array with DGS and absorber.

maximum isolation level achieved is 43 dB at GLONASS G1 band (1.602 GHz). The maximum isolation at the BeiDou B1 band (1.561GHz) is 28 dB while for the GPS L1 and Galileo E1 bands (1.575 GHz), the highest isolation attained is 30 dB. The slight variation in the simulated and measured results is due to the non-idealities of the fabrication process and variation in the permittivity of the substrate. The radiation pattern of the proposed antenna array was measured in the anechoic chamber as shown in Fig. 35. The experimental setup consisted of a 1-4 power divider for feeding the antenna array with equal power at each port.

Fig. 36 shows the measured radiation pattern when a null is formed in the boresight direction at 1.575 GHz. This is the pattern obtained when all four ports are simultaneously excited in the anechoic chamber using a 1-4 power divider. The measured null depth is 48 dB which is in accordance with the simulated results.

TABLE 4. Comparison of proposed antenna with other works.

References	[13]	[19]	[21]	[22]	[23]	[24]	**Proposed**
Area (cm^2)	119.29	122.65	153.20	400	361	196	**122.65**
No. of Antenna Elements	4	4	3	4	4	4	**4**
No. of GNSS bands Covered	L1, L2	L1, B1, E1, G1	L1	L1, B1	B3	B3	**L1, B1, E1, G1**
Isolation level (dB)	> 15, 25	> 20	> 18.6	> 20	> 25	> 18	**> 25**
Gain (dBi)	-	3.3	-	5.4	-	-	**6**
Isolation Enhancement Technique	Meta-material split ring resonator wall	Discontinuous substrate & 9.525 mm thick absorber	Parasitic strips & DGS	-	Meta-material vertical wall of 45 mm height	-	**DGS & 3.175 mm thick absorber**
Design Complexity	High	Low	Moderate	Low	High	High	**Low**

*BDS B3 band is at 1268.52 MHz

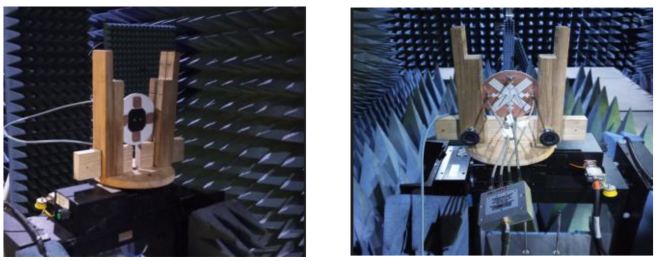

(a) (b)

FIGURE 35. Radiation pattern measurement setup of the proposed DGS and absorber four element antenna array. (a) Front view (b) Back view showing 1-4 power divider.

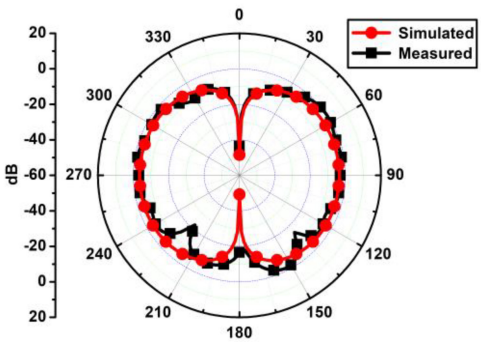

FIGURE 36. Simulated and measured radiation pattern of the proposed array with a null at boresight at 1.575 GHz.

Fig. 34 shows the measured mutual coupling response of the proposed antenna array.

Fig. 37 presents the normalized measured and simulated E and H-plane RHCP and LHCP 2D radiation pattern when only one port is excited at 1.575 GHz showing good polarization purity. Moreover, the nearly hemispherical behaviour of the RHCP radiation pattern with minimum

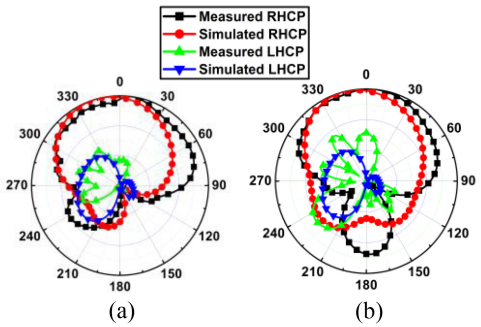

(a) (b)

FIGURE 37. Normalized measured and simulated CP radiation patterns of the proposed array with DGS and absorber at 1.575 GHz. (a) E-plane (b) H-plane.

cross-polarization (LHCP component) and back lobe radiation shows that the proposed antenna array is an excellent choice for robust GNSS upper L-band applications.

Table 4 shows the comparison of proposed of our proposed design with previously reported literature. In comparison with previously published works that cover either one or only two GNSS bands [13], [21], [22], [23], [24], our proposed antenna simultaneously operates on all four GNSS services (BeiDou B1 band 1561.098 MHz, GPS L1 band 1575.42 MHz, Galileo E1 band 1575.42 MHz and GLONASS G1 band 1602 MHz) in the upper L-band. Our proposed design has more isolation level than GNSS arrays reported in [19], [21], [22], [24]. The isolation level reported in [23] is 25 dB, but the size of this array is significantly greater than our proposed array and it operates across only one GNSS band thus making its utility limited. Moreover in [23], a vertical meta-material wall of height 45 mm is used to increase the isolation which increases the design complexity and make it unsuitable for practical applications with strong vibration circumstance. Furthermore, the size of our proposed antenna array is also more compact than designs reported in [21], [22], [24]. In addition to this, our

proposed antenna has a simpler feeding mechanism as compared to the designs that utilize dual feeding networks or lossy lumped components [13], [24], [25], [26]. The size of our proposed antenna is same as reported in [19], but the radiation efficiency and gain of this design is only 38% and 3.3 dBi respectively due to the presence of a 9.525 mm thick MT-30 absorber. We have used only 3.175 mm thick MT-30 absorber which is the least thickness commercially available along with a combination of DGS to enhance the isolation level without degrading the radiation efficiency (> 58.8%) and gain (> 6 dBi). The null depth of our proposed array is also more than reported in [19] due to a higher isolation level of more than 25 dB. Therefore, our proposed four-element antenna array outperforms the previously reported GNSS arrays owing to a greater number of GNSS bands covered, compact size, higher isolation level, more null depth for anti-jamming performance, higher gain, more efficiency and design simplicity.

IV. CONCLUSION

In this work, a compact four element high isolation antenna array is presented for GNSS upper L-band applications. The array is designed on high epsilon material to achieve a compact patch size of only 27.4 mm x 27.4 mm and an overall area of only 122.65 cm^2. The proposed array covers all the four major GNSS services in the upper L-band, i.e., BeiDou B1 (1.561098 GHz), GPS L1 (1.57542 GHz), Galileo EI (1.57542 GHz) and GLONASS G1 (1.602 GHz) by covering the bandwidth from 1.556 -1.610 GHz. A high isolation level of more than 25 dB is achieved in the entire bandwidth of interest by employing a DGS and a low-cost microwave absorber material. The proposed array has a high gain of 6 dBi. The anti-jamming performance of the proposed array is analyzed by the simulating the null depth at the boresight direction which is 48 dB owing to a high isolation level. The MIMO performance parameters ECC (< 0.35) and DG (> 9.3 dB) also have been evaluated for the proposed antenna DGS and absorber array. Owing to a wide bandwidth, high isolation, high gain and better null depth, the proposed array is an excellent choice for GNSS applications.

REFERENCES

[1] C. A. Balanis, *Antenna Theory: Analysis and Design*. Hoboken, NJ, USA: Wiley, 2015.

[2] C. L. Palson, A. E. Sunny, and D. D. Krishna, "Circularly polarized square patch antenna with improved axial ratio bandwidth," in *Proc. IEEE Annu. India Conf. (INDICON)*, 2016, pp. 8–13.

[3] Z. Qamar, L. Riaz, M. Chongcheawchamnan, S. A. Khan, and M. F. Shafique, "Slot combined complementary split ring resonators for mutual coupling suppression in microstrip phased arrays," *IET Microw. Antennas Propag.*, vol. 8, no. 15, pp. 1261–1267, 2014.

[4] W. Kunysz, "Advanced pinwheel compact controlled reception pattern antenna (AP-CRPA) designed for interference and multipath mitigation," in *Proc. 14th Int. Tech. Meeting Satellite Div. Inst. Navigat. (ION GPS)*, Sep. 2001, pp. 2030–2036.

[5] G. Shaker, G. Rafi, S. Safavi-Naeini, and N. Sangary, "A synthesis technique for reducing mutual coupling between closely separated patch antennas," in *Proc. IEEE Antennas Propag. Soc. Int. Symp. (AP-S)*, San Diego, CA, USA, Jul. 2008, pp. 1–4.

[6] A. Diallo, C. Luxey, P. L. Thuc, R. Staraj, and G. Kossiavas, "Study and reduction of the mutual coupling between two mobile phone PIFAs operating in the DCS1800 and UMTS bands," *IEEE Trans. Antennas Propag.*, vol. 54, no. 11, pp. 3063–3074, Nov. 2006.

[7] F. Yang and Y. Rahmat-Samii, "Microstrip antennas integrated with electromagnetic band-gap (EBG) structures: A low mutual coupling design for array applications," *IEEE Trans. Antennas Propag.*, vol. 51, no. 10, pp. 2936–2946, Oct. 2003.

[8] M. Coulombe, K. S. Farzaneh, and C. Caloz, "Compact elongated mushroom (EM)-EBG structure for enhancement of patch antenna array performances," *IEEE Trans. Antennas Propag.*, vol. 58, no. 4, pp. 1076–1086, Apr. 2010.

[9] E. Rajo-Iglesias, O. Quevedo-Teruel, and L. Inclan-Sanchez, "Mutual coupling reduction in patch antenna arrays by using a planar EBG structure and a multilayer dielectric substrate," *IEEE Trans. Antennas Propag.*, vol. 56, no. 6, pp. 1648–1655, Jun. 2008.

[10] D. Chandu, S. Karthikeyan, and K. P. Kumar, "Reduction of mutual coupling in a two element patch antenna array using sub-wavelength resonators," in *Proc. 21st Nat. Conf. Commun.*, 2015, pp. 1–5.

[11] A. Ramachandran, S. V. Pushpakaran, M. Pezholil, and V. Kesavath, "A four-port MIMO antenna using concentric square-ring patches loaded with CSRR for high isolation," *IEEE Antennas Wireless Propag. Lett.*, vol. 15, pp. 1196–1199, 2015.

[12] K. Buell, H. Mosallaei, and K. Sarabandi, "Metamaterial insulator enabled superdirective array," *IEEE Trans. Antennas Propag.*, vol. 55, no. 4, pp. 1074–1085, Apr. 2007.

[13] A. A. Gheethan, P. A. Herzig, and G. Mumcu, "Compact 2 x 2 coupled double loop GPS antenna array loaded with broadside coupled split ring resonators," *IEEE Trans. Antennas Propag.*, vol. 61, no. 6, pp. 3000–3008, Jun. 2013.

[14] A. A. Gheethan and G. Mumcu, "Coupling reduction of coupled double loop GPS antennas using split ring resonators," in *Proc. IEEE Int. Symp. Antennas Propag.*, Jul. 2011, pp. 2613–2616.

[15] K. Wei, J.-Y. Li, L. Wang, Z.-J. Xing, and R. Xu, "Mutual coupling reduction by novel fractal defected ground structure bandgap filter," *IEEE Trans. Antennas Propag.*, vol. 64, no. 10, pp. 4328–4335, Oct. 2016.

[16] M. I. Ahmed, A. Sebak, E. A. Abdallah, and H. Elhennawy, "Mutual coupling reduction using defected ground structure (DGS) for array applications," in *Proc. 15th Int. Symp. Antenna Technol. Appl. Electromagn.*, Jun. 2012, pp. 1–5.

[17] S. Xiao, M.-C. Tang, Y.-Y. Bai, S. Gao, and B.-Z. Wang, "Mutual coupling suppression in microstrip array using defected ground structure," *IET Microw. Antennas Propag.*, vol. 5, no. 12, pp. 1488–1494, Sep. 2011.

[18] E. Everett, A. Sahai, and A. Sabharwal, "Passive self-interference suppression for full-duplex infrastructure nodes," *IEEE Trans. Wireless Commun.*, vol. 13, no. 2, pp. 680–694, Feb. 2014.

[19] M. Awais, A. Madni, and W. T. Khan, "Design of a compact high isolation 4-element wideband patch antenna array for GNSS applications," *IEEE Access*, vol. 10, pp. 13780–13786, 2022.

[20] A. Madni et al., "A compact high isolation wideband MIMO antenna for multi-band applications," *J. Electromagn. Waves Appl.*, vol. 36, no. 14, pp. 2041–2054, 2022.

[21] G. Byun, H. Choo, and S. Kim, "Design of a small arc-shaped antenna array with high isolation for applications of controlled reception pattern antennas," *IEEE Trans. Antennas Propag.*, vol. 64, no. 4, pp. 1542–1546, Apr. 2016.

[22] Y. Liu, S. Zhang, and Y. Gao, "A high-temperature stable antenna array for the satellite navigation system," *IEEE Antennas Wireless Propag. Lett.*, vol. 16, pp. 1397–1400, 2017.

[23] J. Zhang, J. Li, and J. Chen, "Mutual coupling reduction of a circularly polarized four-element antenna array using metamaterial absorber for unmanned vehicles," *IEEE Access*, vol. 7, pp. 57469–57475, 2019.

[24] J. Li, H. Shi, J. Guo, and A. Zhang, "Compact four-element antenna array design for beidou navigation satellite system applications," *Prog. Electromagn. Res. Lett.*, vol. 57, pp. 117–123, Nov. 2015.

[25] Y. Zhou, C. C. Chen, and J. L. Volakis, "Single-fed circularly polarized antenna element with reduced coupling for GPS arrays," *IEEE Trans. Antennas Propag.*, vol. 56, no. 5, pp. 1469–1472, May 2008.

[26] M. Chen and C.-C. Chen, "A compact dual-band GPS antenna design," *IEEE Antennas Wireless Propag. Lett.*, vol. 12, pp. 245–248, 2013.

ABDULLAH MADNI received the B.S. degree in electronic engineering from the Ghulam Ishaq Khan Institute of Engineering Sciences and Technology, Pakistan, in 2015, and the M.S. degree in electrical engineering from the Information Technology University of the Punjab, Pakistan, in 2018. He is currently pursuing the Ph.D. degree in electrical engineering with the Syed Babar Ali School of Science and Engineering, Lahore University of Management Sciences, Pakistan. His main areas of research include design of wide-band antenna arrays for satellite communication, isolation enhancement in antenna arrays, and designing antennas for 5G systems.

WASIF TANVEER KHAN (Senior Member, IEEE) received the B.Sc. degree in electrical engineering from the University of Engineering and Technology, Lahore, Pakistan, in 2005, and the M.S. and Ph.D. degrees in electrical and computer engineering from the Georgia Institute of Technology, Atlanta, USA, in 2010 and 2014, respectively.

From January 2006 to December 2008, he was a Lecturer with the National University of Computer and Emerging Sciences-FAST, Lahore. From January 2015 to January 2023, he worked as an Assistant Professor with the Department of Electrical Engineering, Lahore University of Managements Sciences, Pakistan. Since January 2023, he has been working as an Associate Professor with the Department of Electrical Engineering, National University of Sciences and Technology. He has authored/coauthored more than 70 research papers in peer-reviewed conferences and journals. He was awarded the M.S. Leading to Ph.D. Fulbright scholarship in 2008. Since 2018, he has also been serving as an Associate Editor of *IET Microwaves, Antennas and Propagation*.